Hindawi
Complexity
Volume 2019, Article ID 3769817, 16 pages
https://doi.org/10.1155/2019/3769817

Research Article

Nonlinear Trajectory Controller with Improved Performances for Waveriders

LiuQing Yang,[1,2] YanBin Liu,[3] and Yong Zhang[1,2]

[1]*The Research Institute of Pilotless Aircraft, Nanjing University of Aeronautics and Astronautics, Nanjing 210016, China*
[2]*Key Laboratory of Unmanned Aerial Vehicle Technology of Ministry of Industry and Information Technology, Nanjing University of Aeronautics and Astronautics, Nanjing 210016, China*
[3]*The College of Astronautics, Nanjing University of Aeronautics and Astronautics, Nanjing 210016, China*

Correspondence should be addressed to YanBin Liu; nuaa_liuyanbin@139.com

Received 16 November 2018; Revised 19 January 2019; Accepted 18 February 2019; Published 24 March 2019

Academic Editor: Marcin Mrugalski

This paper presents a nonlinear trajectory controller with improved performances for a general model of the waverider based on feedback linearization theory and composite nonlinear feedback (CNF) technique. First, a nonlinear controller is presented using the dynamic inversion and CNF technique for the MIMO Model, and the robust stability of the proposed controller is proved. Then, the nonlinear model is established on the basis of hypersonic aerodynamic principle, and the dynamic characteristics are analyzed accordingly, and the periodic trajectory is designed and optimized in combination with a fuel optimization problem. Furthermore, the nonlinear controller is applied to the trajectory tracking of the waverider model, and the general design steps are provided the flight controller using this nonlinear control method. Finally, an illustrative example is given to verify the effectiveness of the nonlinear controller of the waverider, and the flight performances are improved accordingly, including system stability, robustness, and tracking ability.

1. Introduction

Air-breathing waveriders are considered a possible means to access space, and these vehicles have commercial and military implications. Unlike rocket-based (combined cycle) systems, air-breathing waveriders can reach orbital speeds without carrying oxygen by applying the scramjet propulsion system [1]. However, waveriders are characterized by extreme aerothermo-elastic-propulsion interactions and uncertainty. As a result, the design of satisfactory control systems for air-breathing waveriders becomes a critical issue to address, with strong couplings between aerodynamic and propulsive effects, while addressing significant uncertainties associated with the complicated flight conditions and special geometries required for these vehicles [2].

For the design of guidance and control systems of air-breathing waveriders, an important task is to construct dynamical models. To this end, a comprehensive analytical model of waverider was developed in [3] using Newtonian impact theory to estimate the pressures that act on the vehicle. Based on the integration of computational fluid dynamics (CFD) and analytical techniques, the stability and control derivatives were determined in [4] to build a model of the longitudinal dynamics of the waverider and investigate the propulsion/airframe integration. A first principle-based dynamic model of the waverider was provided in [5] to incorporate aero-thermo-elastic-propulsion interactions: this model applied inviscid compressible oblique shock-expansion theory to estimate aerodynamic forces and moments, as well as a 1D Rayleigh flow model and an Euler-Bernoulli beam model determined scramjet propulsion and structural flexibility, respectively. Given that the nonlinear physics-based dynamical model in [5] was highly complicated to be employed for control analysis and design, a simplified model of this version was given in [6] to remove a set of weak couplings of nonlinear dynamics. For a comprehensive aero-thermo-elastic-propulsion model of the six-degree-of-freedom dynamics of waverider in [7], a control-oriented model was developed in [8] to allow stability, controllability, and robustness analyses and support the adaptive and

nonlinear control law design. Based on these control-related models of the waverider, some nonlinear controllers have been developed, including the adaptive sliding mode control [9] and linear output feedback tracking control [10].

The control system design of waveriders should be integrated with the guidance law because any small attitude variation leads to a significant change in the trajectory on the hypersonic flight condition. Therefore, feasible trajectory generation is critical for the design of guidance and control of waveriders to improve the flight performance and minimize the control power [11]. The periodic cruise can typically save more fuel than the steady-state cruise in the hypersonic flight phase [12]; thus, applying the periodic flight trajectory helps improve the hypersonic flight performance. Nevertheless, tracking such a trajectory is difficult for the guidance and control system while guaranteeing the respected control qualities, such as fast setting time, small overshot, and robustness during the hypersonic flight. To this end, Parker et al. [13] designed a control system of an air-breathing waverider based on approximate feedback linearization to achieve excellent tracking performance and robustness. Alternatively, a nonlinear adaptive dynamic inversion controller was developed in [14] for a waverider to achieve the desired reference track while being robust to the system uncertainties. The dynamic inversion-based flight control, however, has difficulty in ensuring robustness and good transient performance simultaneously for waveriders [15].

A so-called composite nonlinear feedback (CNF) control technique, presented by Lin et al. [16], can ameliorate transient performances in the control process. Turner et al. [17] applied CNF to higher-order and multiple-input systems. Chen et al. [18] developed a CNF control to a general class of systems with input saturation. This controller consisted of a linear feedback control law and a nonlinear feedback control law without any switching element; as a result, the CNF design can capture the time-optimal maneuver in asymptotically tracking situations [19]. The CNF technique has also been used for nonlinear systems [20], uncertain chaotic systems [21], discrete-time linear systems [22], master/slave synchronization of nonlinear systems [23], and switched systems with input saturation [24]. In particular, a design method of composite nonlinear feedback control technique was presented in [23] for the synchronization of master/slave nonlinear systems, and a new condition was derived for the master and slave systems. Also, a robust tracking problem was considered in [24] for the uncertain switched systems with input saturations, and a new form of the nonlinear function was generated based on a CNF control law to adapt the changes in the tracking targets. Furthermore, a variant factor technique was proposed in [25] to address input saturation in a class of nonlinear systems. If the flight control law is designed with the dynamic inversion and CNF technique, some important control qualities can be improved for waveriders, such as the transient performance and decoupling control capability. Accordingly, this study develops a novel flight control law for a general model of waverider using the CNF technique to guarantee integrated control performances, such as fast setting time, small overshot, and robustness on the hypersonic flight condition. Not only that, the periodic flight trajectory can be followed using this designed controller under uncertain flight conditions, and optimal energy consumption is guaranteed in the course of the waverider flight accordingly.

The rest of this paper is divided into several sections. Section 2 deals with the model properties and periodic cruise trajectory generation of the waverider. Section 3 considers the guidance and control law design for the periodic trajectory using feedback linearization theory and CNF technique. The proof of system stability and robustness is provided accordingly. Section 4 demonstrates an illustrative example, which tests the feasibility of the proposed controller for a general longitudinal model of the waverider. The response performances and fuel consumption savings are compared in relation to the dynamic inversion control and CNF control. Section 5 concludes.

2. Nonlinear Controller with Improved Performances for MIMO Model

A multi-input multioutput (MIMO) affine nonlinear model of waveriders is written with input saturation as follows [26]:

$$\begin{aligned} \dot{x} &= f(x) + \sum_{i=1}^{2} g_i(x)\, sat(u_i) \\ y' &= (h_1(x), h_2(x)) \end{aligned} \tag{1}$$

where $x \in \mathfrak{R}^7$, $y \in \mathfrak{R}^2$, and $u_i \in \mathfrak{R}, i = 1, 2$ are the state, output, and control variables, respectively. *sat* is a function defined as follows:

$$sat(u_i) = \begin{cases} \overline{u}_i, u_i > \overline{u}_i \\ u_i, |u_i| \le \overline{u}_i \\ -\overline{u}_i, u_i < -\overline{u}_i \end{cases} \tag{2}$$

for $i = 1, 2$, where $\overline{u}_i$ is the maximum of u_i. Following that, we give the following assumptions [27].

(1) $f(x) \in \mathfrak{R}^7$ and $g_i(x) \in \mathfrak{R}^7$, $i = 1, 2$ are smooth vector fields and $h_i(x) \in \mathfrak{R}$, $i = 1, 2$ are smooth functions on a compact and connected set X of $\mathfrak{R}^7$.

(2) The relative degree of the nonlinear model is $(r_1, r_2)'$, $r = \sum_{i=1}^{2} r_i$, $r \le 7$, and $r_i \ge 1, i = 1, 2$ on X.

(3) The zero dynamics of the nonlinear model is stable on X if any.

Based on the differential geometry theories, for the nonlinear model there is a nonsingular transformation $\Phi(x)$ from X to $Z \times Z_0$ which is a compact and connected set of $\mathfrak{R}^7$ [28],

$$\begin{pmatrix} z \\ z_0 \end{pmatrix} = \Phi(x), \quad \forall x \in X, \begin{pmatrix} z \\ z_0 \end{pmatrix} \in Z \times Z_0 \tag{3}$$

$$\begin{aligned} \Phi(x) = \Big(& L_f^0 h_1(x), \cdots, L_f^{r_1 - 1} h_1(x), L_f^0 h_2(x), \cdots, \\ & L_f^{r_2 - 1} h_2(x), \phi_{r+1}(x), \cdots, \phi_7(x) \Big) \end{aligned} \tag{4}$$

where

$$L_f^i h_j(x) = f'(x)\frac{\partial L_f^{i-1} h_j(x)}{\partial x} \tag{5}$$

for $i = 1, \cdots, 7$ and $j = 1, 2$,

$$L_f^0 h_j(x) = h_j(x) \tag{6}$$

for $j = 1, 2$,

$$g_j'(x)\frac{\partial \phi_i(x)}{\partial x} = 0 \tag{7}$$

for $i = r+1, \cdots, 7$ and $j = 1, 2$, and $\phi_i(x)$ is a smooth function on X for $i = r+1, \cdots, 7$. According to the nonlinear state transformation $\Phi(x)$, the nonlinear model can be changed as follows:

$$\begin{aligned} \dot{z} &= Az + Bv, \\ z(0) &= z_V \\ v &:= s(z, z_0) + \sum_{i=1}^{2} p_i(z, z_0)\, sat(u_i) \\ y &= Cz \\ \dot{z}_0 &= z_d(z, z_0) \end{aligned} \tag{8}$$

where $z_0 \in \Re^{7-r}$ is the state variable of the zero dynamics and $z \in \Re^r$. In addition, $z_d(z, z_0) \in \Re^{7-r}$ and $s(z, z_0) \in \Re^2$ and $p_i(z, z_0) \in \Re^2$, $i = 1, 2$, are smooth vector fields on $Z \times Z_0$. They are expressed by

$$z_d'(z, z_0) = \left(f'(x)\frac{\partial \phi_{r+1}(x)}{\partial x}, \cdots, f'(x)\frac{\partial \phi_7(x)}{\partial x} \right) \tag{9}$$

$$s'(z, z_0) = \left(f'(x)\frac{\partial L_f^{r_1} h_1(x)}{\partial x}, f'(x)\frac{\partial L_f^{r_2} h_2(x)}{\partial x} \right) \tag{10}$$

$$p_i'(z, z_0) = \left(g_i'(x)\frac{\partial L_f^{r_1} h_1(x)}{\partial x}, g_i'(x)\frac{\partial L_f^{r_2} h_2(x)}{\partial x} \right) \tag{11}$$

$$x = \Phi^{-1}\begin{pmatrix} z \\ z_0 \end{pmatrix} \tag{12}$$

where Φ^{-1} represents the inverse of Φ, which is defined as a nonsingular function from X to $Z \times Z_0$. Accordingly, the system matrices are

$$\begin{aligned} A &= \mathrm{diag}(A_1, A_2) \\ B &= \mathrm{diag}(b_1, b_2) \\ C &= \mathrm{diag}(c_1, c_2) \end{aligned} \tag{13}$$

$$\begin{aligned} A_i &= \begin{bmatrix} 0 & I \\ 0 & 0 \end{bmatrix}, \\ b_i &= \begin{bmatrix} 0 \\ 1 \end{bmatrix}, \\ c_i &= \begin{bmatrix} 1 & 0 \end{bmatrix} \end{aligned} \tag{14}$$

for $i = 1, 2$, where $A_i \in \Re^{r_i \times r_i}$, $b_i \in \Re^{r_i \times 1}$, $c_i \in \Re^{1 \times r_i}$, and I denotes the identify matrix with approximate dimensions.

In addition, a reference generator needs to be designed for the waverider to produce reference in (69) to be tracked, and, based on the equivalent model in (8), it is constructed as follows:

$$\begin{aligned} \dot{\overline{z}} &= A\overline{z} + Bv_e, \\ \overline{z}(0) &= \overline{z}_V \\ v_e &= F_e\overline{z} + r_s \\ r &= C\overline{z} \end{aligned} \tag{15}$$

where $\overline{z} \in \Re^r$ is the state of the reference generator, F_e denotes the feedback gain matrix, r_s represents the virtual signal source, and $\overline{z}_V$ indicates the initial value. This reference generator can produce an arbitrary type of output signal, including the sinusoidal signal and the ramp signal by choosing F_e, r_s, and $\overline{z}_V$.

Furthermore, we will present a CNF control law associated with the reference generator given in the above section in order that the proposed CNF control law can track the designed reference in (15). To this end, we first define $z_e = z - \overline{z}$, and then, based on (8) and (15), we get

$$\begin{aligned} \dot{z}_e &= Az_e + B(v - v_e), \\ v &= s(z, z_0) + \sum_{i=1}^{2} p_i(z, z_0)\, sat(u_i) \\ v_e &= F_e\overline{z} + r_s \\ \widetilde{z} &= y - r = C(z - \overline{z}) = Cz_e \\ \dot{z}_0 &= z_d(z, z_0) \end{aligned} \tag{16}$$

This error equation is applied in the design of the CNF control law, and the detailed design procedure will be introduced in the following steps.

Steps 1. Design a linear feedback control law

$$v_L = Fz_e + v_e \tag{17}$$

where F is the chosen state feedback gain matrix $\Re^{2 \times r}$ such that (1) $A + BF$ is an asymptotically stable matrix and (2) the closed-loop system $C(sI - A - BF)^{-1}B$ has the expected properties. The selection of F is to make the closed-loop poles of $A + BF$ have a dominating pair with a small damping ratio, leading to a fast rise time in the response process.

Steps 2. Given a positive definite symmetric matrix $W \in \Re^{r \times r}$, we solve the following Lyapunov equation:

$$(A + BF)'P + P(A + BF) = -W \tag{18}$$

for $P > 0$. Accordingly, the nonlinear feedback portion of the CNF control law u_N is provided by

$$v_N = \rho B'Pz_e \tag{19}$$

where $\rho = \mathrm{diag}(\rho_1, \rho_2)$, and ρ_i, $i = 1, 2$, represent the nonpositive functions regarding z_e, which are used to gradually adjust the damping ratio of the closed-loop system to obtain better tracking performance.

Steps 3. The linear feedback control law and nonlinear feedback part are constituted to get a generalized CNF control law:

$$v = v_L + v_N = Fz_e + v_e + \rho B' P z_e \tag{20}$$

Steps 4. The control law for the equivalent linear model is designed as follows:

$$u : \begin{pmatrix} u_1 \\ u_2 \end{pmatrix} = p^{-1}(z, z_0)\left[Fz_e + v_e + \rho B' P z_e - s(z, z_0)\right] \tag{21}$$

Furthermore, for a set of scalars $\tau_i \in (0, 1)$, $i = 1, 2$, let $\mu > 0$ be the largest positive scalar such that, for all $x \in X_{iV}$, where

$$X_{iV} \coloneqq \left\{x : x' P x \le \mu\right\}, \tag{22}$$

the following condition holds:

$$m_i \|Fx\| \le (1 - \tau_i)\,\overline{u}_i, \quad i = 1, 2 \tag{23}$$

$$m_i = \max_{x \in X} \left\| e_i' p^{-1}(z, z_0) \right\| \tag{24}$$

where m_i is not zero as p is invertible, and $e_i' \in \Re^2$ is a vector in which only the i-th element of e_i is 1 and the other is zero.

Beyond this, for getting further results, first we propose a lemma below.

Lemma 1. *Suppose that* $q_z = \mathrm{diag}(q_{z1}, q_{z2})$*, and, then,*

$$\lambda_{\min}\left[p_\rho q_z p_\rho^{-1} + \left(p_\rho'\right)^{-1} q_z p_\rho'\right] = 2\min(q_{z1}, q_{z2}) \tag{25}$$

where $\lambda_{\min}$ *denotes the minimal eigenvalue.*

Proof. As $p_\rho q_z p_\rho^{-1} + (p_\rho')^{-1} q_z p_\rho'$ is a symmetric matrix,

$$\begin{aligned} &\lambda_{\min}\left[p_\rho q_z p_\rho^{-1} + \left(p_\rho'\right)^{-1} q_z p_\rho'\right] \\ &= \min_{\|x\|=1} x'\left[p_\rho q_z p_\rho^{-1} + \left(p_\rho'\right)^{-1} q_z p_\rho'\right] x \\ &= \min_{\|x\|=1} 2x' p_\rho q_z p_\rho^{-1} x \end{aligned} \tag{26}$$

Afterwards, we provide a Lagrange function as follows:

$$L_z = 2x' p_\rho q_z p_\rho^{-1} x + 2\lambda_z\left(1 - x'x\right) \tag{27}$$

where $2\lambda_z$ is the Lagrange multiplier. Following that

$$\begin{aligned} &\frac{\partial L_z}{\partial x} = 4p_\rho q_z p_\rho^{-1} x - 4\lambda_z x = 0, \Longrightarrow \\ &p_\rho\left(q_z - \lambda_z I\right) p_\rho^{-1} x = 0 \end{aligned} \tag{28}$$

$$\begin{aligned} &\frac{\partial L_z}{\partial \lambda_z} = 2\left(1 - x'x\right) = 0, \Longrightarrow \\ &x'x = 1 \end{aligned} \tag{29}$$

Actually, if $\lambda_z \ne q_{zi}$, there is no stationary point. As $\lambda_z = q_{zi}$, there is one stationary point, $x'x = 1$, and $p_\rho q_z p_\rho^{-1} x_i = q_{zi} x_i$ so that

$$2x_i' p_\rho q_z p_\rho^{-1} x_i = 2q_{zi} \tag{30}$$

Thus,

$$\begin{aligned} \lambda_{\min}\left[p_\rho q_z p_\rho^{-1} + \left(p_\rho'\right)^{-1} q_z p_\rho'\right] &= \min_{\|x\|=1} 2x' p_\rho q_z p_\rho^{-1} x \\ &= 2\min(q_{z1}, q_{z2}) \end{aligned} \tag{31}$$

This completes proof of Lemma 1, and the result of Lemma 1 will be applied in the proof of the following Theorem. □

Theorem 2. *Suppose that*

(1) $f(x)$ *and* $g_i(x)$, $i = 1, 2$ *are smooth vector fields and* $h_i(x)$, $i = 1, 2$ *are smooth function on a compact and connected set* X *of* $\Re^7$.

(2) *The relative degree of the nonlinear model is* $(r_1, r_2)'$, $r = r_1 + r_2 \le 7$, *and* $r_i \ge 1$, $i = 1, 2$ *on* X.

(3) *Zero dynamics of the nonlinear model in (1) is stable on* X *if any.*

(4) $p(z, z_0) = (p_1(z, z_0), p_2(z, z_0))$ *is invertible at* $\forall \binom{z}{z_0} \in Z \times Z_0$ *in which* $\binom{z}{z_0} = \Phi(x)$ *is nonsingular on* X.

Then, with the CNF control law comprising (18) and (21) will drive system output y *to track arbitrary reference* r *from an initial state asymptotically without steady-state error, provided that the following properties are satisfied.*

(1) *There exist a set of scalars,* $\tau_i \in (0, 1)$, $i = 1, 2$, *so that*

$$\left\| e_i' p^{-1}(z, z_0)\left[v_e - s(z, z_0)\right] \right\| \le \tau_i \overline{u}_i, \quad i = 1, 2 \tag{32}$$

(2) $\rho(z_e) = \mathrm{diag}(\rho_1, \rho_2)$ *and*

$$\rho_i \le 0 \tag{33}$$

for $i = 1, 2$.

(3) *Let* x_{iV} *be the initial value of* x. *Then, the initial condition* z_{eV} *of* z_e *satisfies*

$$z_{eV} \in X_{iV}, \quad \begin{pmatrix} z_{eV} \\ z_{0,V} \end{pmatrix} = \Phi\left(X_{iV}\right) \tag{34}$$

Proof. Consider $z_e = z - \overline{z}$; then

$$\begin{aligned} u &= p^{-1}(z, z_0)\left[Fz_e + v_e + \rho B' P z_e - s(z, z_0)\right] \\ &= p^{-1}(z, z_0)\,\rho B' P z_e + p^{-1}(z, z_0) Fz_e \\ &\quad + + p^{-1}(z, z_0)\left[v_e - s(z, z_0)\right] \end{aligned} \tag{35}$$

When $z_e \in X_{iV}$, it shows that

$$m_i \|Fz_e\| \le (1 - \tau_i)\,\overline{u}_i, \quad i = 1, 2 \tag{36}$$

Thus,

$$\begin{aligned} \left\| e_i' p^{-1}(z, z_0) Fz_e \right\| &\le \left\| e_i' p^{-1}(z, z_0) \right\| \|Fz_e\| \\ &\le m_i \|Fz_e\| \le (1 - \tau_i)\,\overline{u}_i \end{aligned} \tag{37}$$

Afterwards, with (32) and (37), we have

$$\begin{aligned}&\left\|e_i' p^{-1}(z,z_0) F z_e + e_i' p^{-1}(z,z_0)\left[v_e - s(z,z_0)\right]\right\| \\ &\quad \le \left\|e_i' p^{-1}(z,z_0) F z_e\right\| \\ &\qquad + \left\|e_i' p^{-1}(z,z_0)\left[v_e - s(z,z_0)\right]\right\| \\ &\quad \le (1-\tau_i)\,\overline{u}_i + \tau_i \overline{u}_i = \overline{u}_i\end{aligned} \tag{38}$$

Following that, the input channels with the saturation can be expressed by [21]:

$$sat(u) = p^{-1}(z,z_0) F z_e + p^{-1}(z,z_0)(v_e - s) + \omega \tag{39}$$

where $\omega = q_z p^{-1} \rho B' P z_e$, $q_z = \mathrm{diag}(q_{z1}, q_{z2})$, and $q_{zi} \in [0,1]$ for $i = 1, 2$. Substituting (39) into (16), we have

$$\dot{z}_e = A z_e + B\left(F z_e + p\omega\right) \tag{40}$$

As a result, the closed-loop system involving (16) and (40) can be expressed by

$$\begin{aligned}\dot{z}_e &= (A + BF) z_e + Bp\omega \\ \dot{z}_0 &= z_d(z, z_0)\end{aligned} \tag{41}$$

The above equation is combined with two parts and the second part is assumed to be stable for the zero dynamics, so only stability of the first part needs to be proved accordingly.

Based on that, we choose a Lyapunov function below

$$\Gamma = z_e' P z_e \tag{42}$$

Then, the derivative of Γ can be calculated with (18) and (41) as follows:

$$\begin{aligned}\dot{\Gamma} &= \dot{z}_e' P z_e + z_e' P \dot{z}_e \\ &= -z_e' W z_e \\ &\quad + z_e' P B\left[\rho\left(p'\right)^{-1} q_z p' + p q_z p^{-1} \rho\right] B' P z_e\end{aligned} \tag{43}$$

Let $\varepsilon > 0$ be a tiny number, so (43) is rewritten as

$$\begin{aligned}\dot{\Gamma} &= -z_e' W z_e \\ &\quad - z_e' P B R_p\left[\left(p_\rho'\right)^{-1} q_z p_\rho' + p_\rho q_z p_\rho^{-1}\right] R_p B' P z_e \\ &\quad + \varepsilon z_e' P B\left[\left(p'\right)^{-1} q_z p' + p q_z p^{-1}\right] B' P z_e\end{aligned} \tag{44}$$

where $R_p = (-\rho + \varepsilon I)^{1/2}$ and $p_\rho = R_\rho^{-1} p$.

Evidently, based on Lemma 1, the second item of (44) is expressed as follows:

$$\begin{aligned}&- z_e' P B R_p\left[\left(p_\rho'\right)^{-1} q_z p_\rho' + p_\rho q_z p_\rho^{-1}\right] R_p B' P z_e \\ &\quad \le -z_e' P B R_p 2\min(q_{z1}, q_{z2}) R_p B' P z_e \le 0\end{aligned} \tag{45}$$

Furthermore, the third item of (44) is shown as

$$\begin{aligned}&\varepsilon z_e' P B\left[\left(p'\right)^{-1} q_z p' + p q_z p^{-1}\right] B' P z_e \\ &\quad = \varepsilon z_e' P B 2\lambda_z B' P z_e\end{aligned} \tag{46}$$

where $\min(q_{z1}, q_{z2}) \le \lambda_z \le \max(q_{z1}, q_{z2})$; that is, $\lambda_z \in [0,1]$. Thus, (44) is expressed by

$$\begin{aligned}\dot{\Gamma} &\le -z_e' W z_e + \varepsilon z_e' P B 2\lambda_z B' P z_e \\ &\le -\sigma_{\min}(W) z_e' z_e + 2\varepsilon\sigma_{\max}\left(P B B' P\right) z_e' z_e\end{aligned} \tag{47}$$

Obviously, $\varepsilon < 0.5\sigma_{\min}(W)\sigma_{\max}^{-1}(PBB'P)$ exists; therefore,

$$\dot{\Gamma} \le -\sigma_{\min}(W) z_e' z_e + 2\varepsilon\sigma_{\max}\left(P B B' P\right) z_e' z_e < 0 \tag{48}$$

These results indicate that once $z_{eV} \in X_{iV}$, z_{eV} will never be out of X_{iV} as $\dot{\Gamma} < 0$ if (22), (23), (24), and (34) are met. In other words, the initial value of z_{eV} is satisfied with $z_{eV} \in X_{iV}$; z_{eV} will lie in X_{iV} based on $\dot{\Gamma} < 0$. Therefore, the closed-loop system including (16) and (21) is asymptotically stable. This accomplishes the proof of this Theorem. □

Remark. the equivalent form of (41) is expressed as

$$\dot{z}_e = A_c z_e + B W_a \tag{49}$$

where $A_c = A + BF$ and $W_a = p\omega$. Based on the results in [28], the stability of the closed-loop system matrix A_c in the region of linear matrix inequality (LMI) is satisfied with

$$L \otimes P + O \otimes \left(\mathbf{A}_c P\right) + Q^T \otimes \left(A_c P\right)^T < 0 \tag{50}$$

where the symmetric matrix L, P and matrix Q make $\Omega = \{s \in C : \mathbf{L} + s\mathbf{Q} + \overline{s}\mathbf{Q}^T < 0\}$. Accordingly, Ω indicates a LMI region. Therefore, the adjusted function ρ can ensure the system asymptotic stability to meet the stability condition of Linear Matrix Inequalities (LMIs) accordingly.

To be specific, the main task of adding the nonlinear part is to alter the damping ratios of the closed-loop system as the outputs approach the periodic cruise trajectory commands, and the nonlinear gains can help to improve stability robustness and to suppress the effect of uncertainties in accordance with the adaptive regulation ability.

3. Nonlinear Trajectory Controller for Waveriders

This study investigates the design methods of the track controller using CNF technique as the waverider flies along with the periodic cruise trajectory. The vehicle shape chosen for this study is shown in Figure 1, where the vehicle geometry is assumed to have unity depth [5].

Figure 1 illustrates the basic geometry of the waverider. A combination of oblique shock and Prandtl-Meyer flow theory is used to determine the pressures on the vehicle surfaces, whereas a 1D Rayleigh flow scramjet propulsion

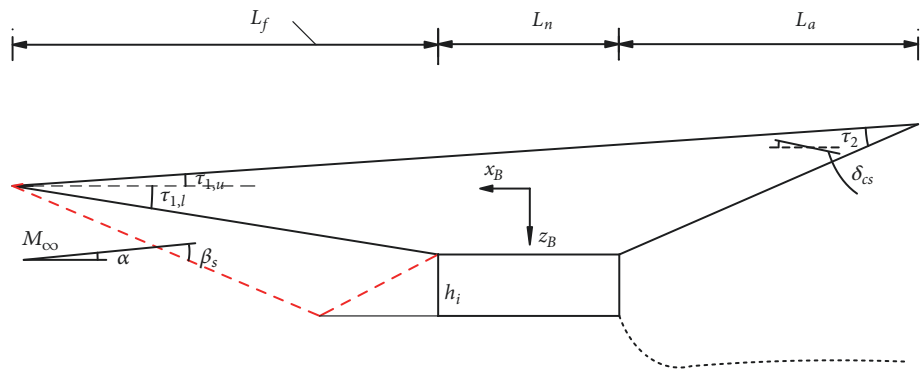

Figure 1: Representative shape of waverider.

model is applied with a variable geometry inlet. Specifically, an oblique shock occurs on the lower forebody as $\alpha \geq -\tau_{1,l}$. The respective airflow properties across the bow shock are determined by [29]:

$$\tan\left(\tau_{1,l}+\alpha\right)=\frac{2\cot\beta_s\left(M_\infty^2\sin^2\beta_s-1\right)}{M_\infty^2\left(\gamma_c+1-2\sin^2\beta_s\right)+2} \tag{51}$$

$$M_1\sin\left(\beta_s-\tau_{1,l}-\alpha\right)=\sqrt{\frac{1+\left(\left(\gamma_c-1\right)/2\right)M_\infty^2\sin^2\beta_s}{\gamma_c M_\infty^2\sin^2\beta_s-\left(\gamma_c-1\right)/2}} \tag{52}$$

$$\frac{P_1}{P_\infty}=1+\frac{2\gamma_c}{\gamma_c+1}\left(M_\infty^2\sin^2\beta_s-1\right) \tag{53}$$

where γ_c is the specific heat ratio for air, β_s denotes the shock wave angle, α indicates the angle of attack, M_∞ and M_1 represent the flight Mach on the front and rear of the shock wave, respectively, and P_∞ and P_1 indicate the pressures on the front and rear of the shock wave, respectively. Similarly, a Prandtl-Meyer expansion occurs on the upper surface as $\alpha \leq -\tau_{1,u}$, and the relations between the geometric parameters and aerodynamic characteristics are decided by [30]:

$$\nu\left(M_\infty\right)=\sqrt{\frac{\gamma_c+1}{\gamma_c-1}}\left\{\tan^{-1}\sqrt{\frac{\gamma_c-1}{\gamma_c+1}\left(M_\infty^2-1\right)}\right\}-\tan^{-1}\sqrt{M_\infty^2-1} \tag{54}$$

$$\nu\left(M_1\right)=\nu\left(M_\infty\right)+\tau_{1,u}+\alpha \tag{55}$$

$$\frac{P_1}{P_\infty}=\left[\frac{1+\left(\left(\gamma_c-1\right)/2\right)M_\infty^2}{1+\left(\left(\gamma_c-1\right)/2\right)M_1^2}\right]^{\gamma_c/(\gamma_c-1)} \tag{56}$$

Once the pressures acting on all vehicle surfaces are computed based on either oblique shock theory or Prandtl-Meyer expansion flow theory, the aerodynamic forces such as the lift L, drag D, and pitch moment M_y can be determined. Aside from these aerodynamic forces, the propulsive force T is calculated according to the momentum theorem from fluid mechanics and expressed by [31]

$$T=\dot{m}_a\left(V_e-V_\infty\right)+\left(P_e-P_\infty\right)A_e-\left(P_1-P_\infty\right)A_i \tag{57}$$

where A_e and A_i indicate the exit area and inlet area of the propulsive system, respectively, P_e and V_e denote the exhaust exit pressure and velocity, respectively, and $\dot{m}_a$ is the mass flow of air, which is determined by [32]:

$$\eta_c\dot{m}_f H_f=\dot{m}_a\left(h_{t3}-h_{t2}\right)+\dot{m}_f h_{t3} \tag{58}$$

$$\dot{m}_f=\beta f_{st}\dot{m}_a \tag{59}$$

where h_{t2} and h_{t3} denote the total enthalpy at the combustor inlet and exit, respectively, β and $\dot{m}_f$ are the equivalence ratio and mass flow of fuel, respectively, η_c represents the combustor efficiency, and f_{st} and H_f indicate the stoichiometric fuel-air ratio and fuel lower heating value for the given fuel, respectively.

When the lift L, drag D, pitch moment M_y, and thrust T are acquired, the longitudinal model of the waverider along with the velocity coordinate system is provided by [33]:

$$\begin{aligned}\dot{V}&=\frac{T\cos\alpha-D}{m}-g\sin\gamma\\ \dot{\gamma}&=\frac{L+T\sin\alpha}{mV}-\frac{g\cos\gamma}{V}\\ \dot{h}&=V\sin\gamma\\ \dot{\alpha}&=q-\dot{\gamma}\\ \dot{q}&=\frac{M_y}{\mathrm{I}_y}\end{aligned} \tag{60}$$

where V denotes the flight velocity, γ is the flight path angle, q represents the pitch angle velocity, α indicates the angle of attack, h is the flight height, and r denotes the flight range, which is determined by $\dot{r}=V\cos\gamma$. In addition, m, g, and I_y are the airplane mass, gravitational constant, and moment of inertia, respectively. For (60), the elevon deflection angle δ_e and equivalence ratio Φ are chosen as the control inputs, and then, based on the aforementioned force computation

theories, the lift L, drag D, pitch moment M_y, and thrust T can be expressed as functions regarding the flight states and inputs by

$$\begin{aligned} L &= 0.5\rho V^2 S C_L(\alpha, \delta_e) \\ D &= 0.5\rho V^2 S C_D(\alpha, \delta_e) \\ M_y &= 0.5\rho V^2 S\bar{c} C_M(\alpha, \delta_e) \\ T &= f_T(\alpha, \delta_e, \beta) \end{aligned} \tag{61}$$

where S and $\bar{c}$ indicate the reference area and mean aerodynamic chord, respectively, ρ represents air density, and C_L, C_D, and C_M denote the coefficients with regard to the lift, drag, and pitch moment, respectively.

We consider the classical short-period approximation by applying the Jacobian linearization for (60) and (61). The transfer function between the flight path angle and elevator deflection is approximately described as [33]:

$$\frac{\Delta\gamma}{\Delta\delta_e} = \frac{C_\gamma\left(s + 1/T_{\gamma 1}\right)\left(s + 1/T_{\gamma 2}\right)\left(s - 1/T_{\gamma 2}\right)}{\left(s + T_{\delta 1}\right)\left(s + T_{\delta 2}\right)} \tag{62}$$

where

$$T_{\delta 1}, T_{\delta 2} = \frac{Z_\alpha}{2V_t} \pm \frac{\sqrt{\left(Z_\alpha - V_t M_q\right)^2 + 4V_t^2 M_\alpha}}{2V_t} \tag{63}$$

$$\frac{1}{T_{\gamma 2}} = \sqrt{M_\alpha - \frac{M_{\delta_e}}{Z_{\delta_e}} Z_\alpha} \tag{64}$$

where $M_\alpha = (1/I_y)(\partial M_y/\partial\alpha)$, $M_q = (1/I_y)(\partial M_y/\partial q)$, $M_{\delta_e} = (1/I_y)(\partial M_y/\partial\delta_e)$, $Z_\alpha = -(1/m)(\partial L/\partial\alpha)$, and $Z_{\delta_e} = -(1/m)(\partial L/\partial\delta_e)$. In addition, C_γ represents the transfer function gain, and the subscript t denotes the trim value. For the basic geometry of waverider in Figure 1, $M_\alpha > 0$ because of the large force acted on the lower surface, which presents an unstable pole according to (63), thereby leading to unstable short-period dynamics for the longitudinal model of the waverider [5]. In addition, the lift corresponding to the elevator deflection results in the existence of a nonminimum phase zero because of $Z_{\delta_e} < 0$. Fortunately, Z_{δ_e} is very small because of the flight in the very low density environment, such that this nonminimum phase zero locates at the far right. In sum, the model dynamics of waverider are unstable, nonminimum, and strong coupling and present large uncertain disturbances and unknown model dynamics. As a result, designing a satisfactory guidance and control system for waverider is a challenging task.

In this section, a guidance and control law using the dynamic inversion and CNF technique is derived for the waverider to track the optimized periodic cruise trajectory. This proposed design process integrates the guidance and control loops by merging the attitude, velocity, and altitude dynamics of the waverider.

The established nonlinear model of waverider in (60) and (61) is difficult to use for some nonlinear control techniques because the obtained lift, drag, and moment are nonanalytical. As a result, the control law design must conduct the model simplification associated with the design requirements. The critical dynamic characteristics concerning the initial model should be retained, although it is simplified to be analytically tractable. Thus, the core work in the model simplification course aims to identify the analytical expressions of the lift, drag, thrust, and pitching moment that need to not only conform to the initial model features but also be in accordance with the control-oriented design goal.

In this study, the forms for the force and moment functions in (61) are selected as [6]:

$$\begin{aligned} C_L(\alpha, \delta_e) &= C_L^{\alpha^2}\alpha^2 + C_L^{\alpha}\alpha + C_L^{\alpha\delta_e}\alpha\delta_e + C_L^{\delta_e^2}\delta_e^2 \\ &\quad + C_L^{\delta_e}\delta_e + C_L^0 \\ C_D(\alpha, \delta_e) &= C_D^{\alpha^2}\alpha^2 + C_D^{\alpha}\alpha + C_D^{\alpha\delta_e}\alpha\delta_e + C_D^{\delta_e^2}\delta_e^2 \\ &\quad + C_D^{\delta_e}\delta_e + C_D^0 \\ C_M(\alpha, \delta_e) &= C_M^{\alpha^2}\alpha^2 + C_M^{\alpha}\alpha + C_{M,\alpha}^0 + c_e\delta_e \\ T &\approx C_T^{\alpha^3}\alpha^3 + C_T^{\alpha^2}\alpha^2 + C_T^{\alpha}\alpha + C_T^0 \end{aligned} \tag{65}$$

where

$$\begin{aligned} C_T^{\alpha^3} &= \varepsilon_1(h, Q)\beta + \varepsilon_2(h, Q) \\ C_T^{\alpha^2} &= \varepsilon_3(h, Q)\beta + \varepsilon_4(h, Q) \\ C_T^{\alpha} &= \varepsilon_5(h, Q)\beta + \varepsilon_6(h, Q) \\ C_T^0 &= \varepsilon_7(h, Q)\beta + \varepsilon_8(h, Q) \end{aligned} \tag{66}$$

where $Q = 0.5\rho V^2$ is dynamic pressure and $C_L^{\alpha^2}$, C_L^{α}, $C_L^{\alpha\delta_e}$, $C_L^{\delta_e^2}$, $C_L^{\delta_e}$, and C_L^0 denote the needed identification parameters for the lift terms. The item parameters for the drag, pitching moment, and thrust also have to be acquired. The scramjet of the waverider strongly depends on the angle of attack and dynamic pressure along with the input Φ. The flight attitude is also dramatically influenced by the propulsive action because of the airflow compression and expansion at the inlet and outlet, which leads to the significant change in the lift and drag. As a result, the mutual effects between the flight attitude change and propulsive action bring a significant challenge for the design of the guidance and control system.

In further implementation, the parameters of the polynomial functions in (65) and (66) are acquired using the least-squares approach based on the model datum derived from the anterior estimation approaches concerning the aerodynamic and propulsive forces. Theoretically, these parameters that have considerable coupling items may result in fairly accurate fitting results, but the complexity of these functions is unfavorable for the guidance and control law design. Thus, from the perspective of the control design for the waverider, we need a compromise selection of the function forms in (65) and (66).

To design the integrated guidance and control law in the preceding part, the outputs of the nonlinear model in (60), (61), and (65) are selected as $y_1 = V$ and $y_2 = h$. In addition, a second-order actuator model is added to the input β, and the propulsive commanded value β_c is selected as the new control input; that is,

$$\ddot{\beta} = -2\xi_T\omega_T\dot{\beta} - \omega_T^2\beta + \omega_T^2\beta_c \tag{67}$$

where ξ_T and ω_T represent the damping ratio and natural frequency of the actuator, respectively. Thus, the control inputs are changed as $u_1 = \beta_c$ and $u_2 = \delta_e$. Furthermore, we choose the flight state vector as $x = [V, \gamma, h, \alpha, q, \beta_c, \dot{\beta}_c]'$ such that the nonlinear model in combination with (60) and (67) becomes a 7D model; that is, this model has a relative degree of 7 over the operating range of interest.

The application of periodic cruise trajectories for hypersonic flight can achieve better fuel consumption savings than that of the steady-state cruise trajectories because of the more effective kinetic-potential energy interchange of the former [14]. However, designing and tracking such periodic cruise trajectories are more difficult and complicated than the process for the steady-state trajectories. Therefore, planning and optimizing the feasible periodic trajectories are critical to improve the cruise performances for waverider.

For the steady-state trajectories, once the model properties, environmental parameters, and aerodynamic expressions are determined, the corresponding trim values with regard to the given velocity and altitude can be solved by

$$\begin{aligned} T_t\cos\alpha_t - D_t &= 0 \\ L_t + T_t\sin\alpha_t - mg &= 0 \\ M_{yt} &= 0 \end{aligned} \tag{68}$$

For the periodic cruise trajectories, how to acquire considerable performance benefit needs to be discussed in view of fuel consumption savings. Compared with the steady-state trajectories, where the engine is always switched on, the periodic cruise trajectories allow the waverider to switch off its engine at some points. For simplicity, we consider that the engine works as $\gamma > 0$ when the vehicle continues to climb. In turn, the engine turns off in the descent phase. We further adopt a parameterized periodic trajectory in [34], which is given by

$$h = h_t + \exp\left[-\eta\left(\frac{r}{r_f}\right)\right]\left[h_a\sin\left(\frac{2\pi r}{r_f}\right)\right] \tag{69}$$

$$\frac{dV}{dr} = \frac{T\cos\alpha - D - mg\sin\gamma}{mV\cos\gamma} \tag{70}$$

$$\frac{dh}{dr} = \tan\gamma \tag{71}$$

$$\frac{d\gamma}{dr} = \frac{L + T\sin\alpha - mg\cos\gamma}{mV^2\cos\gamma} \tag{72}$$

where h_a is the amplitude of the periodic trajectory, η denotes the damping term, and r_f indicates the period parameter regarding the flight range. h_a, η, and r_f are the adjusted parameters that should be optimized to minimize the following cost function [14]:

$$J = \frac{\int_0^{T_z}\dot{m}_f dt}{\int_0^{T_z}\dot{r}dt} \tag{73}$$

where T_z is the total flight time. This cost function minimizes the ratio of the fuel consumption over the flight range. According to the parameterized periodic trajectory in (69), the dynamic balance values can be computed by

$$\begin{aligned} T_t\cos\alpha_t - D_t - mg\sin\gamma_t &= 0 \\ mV_t\dot{\gamma}_t &= L + T\sin\alpha_t - mg\cos\gamma_t \\ M_{yt} &= 0 \\ \left(\frac{\partial h}{\partial r}\right)_t &= \tan\gamma_t \end{aligned} \tag{74}$$

where

$$\begin{aligned} \left(\frac{\partial h}{\partial r}\right)_t = {} & \left(-\frac{\eta}{r_f}\right)\exp\left[-\eta\left(\frac{r}{r_f}\right)\right]\left[h_a\sin\left(\frac{2\pi r}{r_f}\right)\right] \\ & + \left(\frac{2\pi}{r_f}\right)\exp\left[-\eta\left(\frac{r}{r_f}\right)\right]\left[h_a\cos\left(\frac{2\pi r}{r_f}\right)\right] \end{aligned} \tag{75}$$

$$\begin{aligned} \dot{\gamma}_t = {} & \cos^2\gamma_t\left[h_a\sin\left(\frac{2\pi r}{r_f}\right)\right] \\ & \cdot\exp\left[-\eta\left(\frac{r}{r_f}\right)\right]\left[\frac{\left(\eta^2 - 4\pi^2\right)}{r_f^2}\right] \\ & - \cos^2\gamma_t\left[h_a\cos\left(\frac{2\pi r}{r_f}\right)\right]\exp\left[-\eta\left(\frac{r}{r_f}\right)\right] \\ & \cdot\left(\frac{4\pi\eta}{r_f^2}\right) \end{aligned} \tag{76}$$

Based on (74), (75), and (76), the dynamic trim states can be obtained in relation to each flight speed and altitude. If the periodic trajectory is given, then the reference command associated with the guidance and control action is decided. The optimal periodic cruise problem in (73) is too complex to be solved analytically; thus, it is solved numerically in this study using the genetic algorithm toolbox in MATLAB. Once the optimal values are obtained, we design the guidance and control law for the waverider to follow this optimized reference trajectory.

Furthermore, the nonlinear controller in Section 1 is employed to the model-based optimized reference trajectory of the waverider, and the structure diagram of the trajectory controller using CNF technique is provided for the waverider in Figure 2.

Figure 2 shows that the presented controller combines the CNF technique with the inversion control structure for

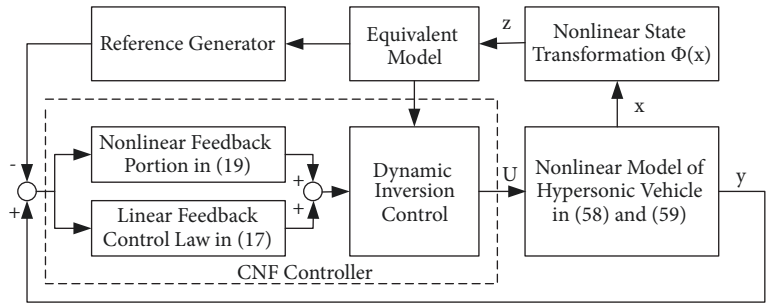

Figure 2: Structure diagram of guidance and control design using CNF technique for hypersonic vehicle.

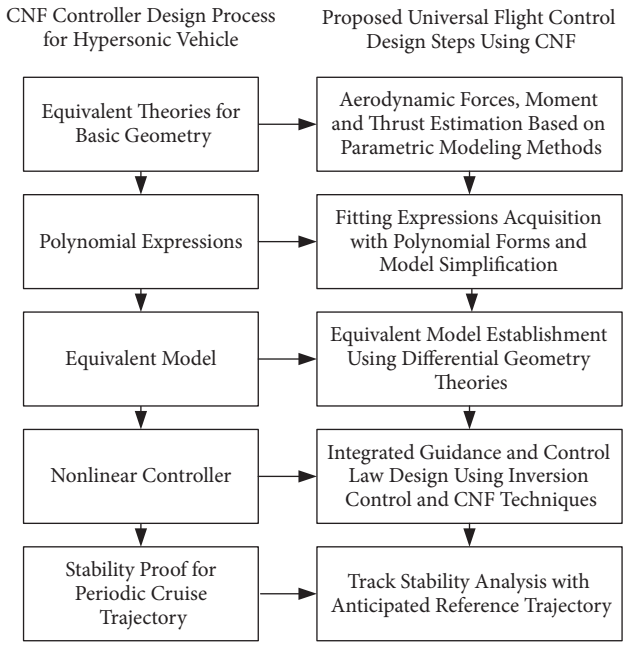

Figure 3: General design steps for flight control law Using CNF technique.

the waverider. To be specific, the nonlinear model is first converted into the resulting equivalent model based on the differential geometry theories. Then, a linear feedback control law is designed to become a closed-loop system with faster rise time. Afterwards, the nonlinear feedback control law is applied to reduce overshoot and improve transient performance in tracking control. Not only that, a combination of the linear and nonlinear feedback control will guarantee closed system stability and robustness in the presence of the unknown model dynamics, while repressing the uncertain disturbances in the complicated flight environment.

The selection of the design parameters W and ρ in (18) and (19) is important to improve transient performance in tracking control, and this is because the nonlinear part of CNF controller will assist speeding up the settling time and decreasing the overshoot, or, equivalently, contributing to a large part to the control input as the tracking errors are small. Basically, the poles of the closed-loop system can be adjusted by the functions ρ_i as a result that these poles approach the invariant zeros of the auxiliary system which is similarly defined in [20] as $|\rho_i|$ become larger and large. In fact, the larger $|\rho_i|$ will lead to a larger damping ratio and yield a smaller overshoot, so one possible choice of ρ_i is provided as follows:

$$\rho_i = -\varepsilon_i \left| e^{-\tau_i |e_i|} - e^{-\tau_i |y_i - r_i|} \right|, \quad i = 1, 2 \tag{77}$$

where ε_i and τ_i are chosen positive scalars to yield a desired track performance. Evidently, when the track error e_i is large, the effect of the nonlinear part of the CNF controller is limited due to the small value of ρ_i, whereas the nonlinear part will be effective as e_i is small. Finally, we note that the choice of ρ_i is nonunique, and any function will work as if it has similar characteristics of that given in (77).

Besides the given guidance and control law design of waverider, the CNF control methods are also considered a general strategy for flight control. Correspondingly, the flow diagram with regard to the design steps using the CNF technique is provided in Figure 3.

According to Figure 3, the general design steps for the flight control law design are provided as follows.

Steps 1. The database of the aerodynamic forces and thrust is built based on the CFD and engineering estimation methods. The obtained aerodynamic forces and thrust are input into the nonlinear airplane model. A full simulation model derived from first principles is established to verify the presented control designs.

Steps 2. Based on the acquired databases, the polynomial expressions regarding aerodynamic forces and thrust are identified using fitting approaches. A curve-fitted model is accordingly obtained. The inherent dynamics of this model with the fitting expressions is compared with the full simulation model to demonstrate the effectiveness of the model simplification mean.

Steps 3. After determining the simplified model with the polynomial expressions, we obtain the resulting equivalent model using differential geometry theories. Unlike the Jacobian linear structure with the given flight point, the feedback linearization method can maintain the nonlinear model dynamics, broaden the resulting structure over a large

flight range, and be combined with some advanced control methods.

Steps 4. The guidance and control law with linear feedback and a nonlinear control part is designed using the CNF technique and inversion control structure. This proposed guidance and control system can track general target reference trajectories with input saturation. The respected flight qualities, including fast setting time, small overshot, and robustness, are ensure.

In general, the developed guidance and control law using the CNF technique is generally suitable for the nonlinear model of any fixed-wing vehicle to track arbitrary flight trajectories in line with the aforementioned step-by-step design procedure. This process depends on the control-oriented model with the curve-fitted mean instead of the linear model with the Jacobian linearization while driving the applicability of the CNF technique in combination with the dynamic inversion control. As a result, this proposed controller can ameliorate transient performance in tracking the anticipated reference trajectories and guarantee system robustness.

4. Illustrative Example

This study adopts the typical waverider geometry of waverider in [5] to validate the feasibility of the proposed control law. This configuration makes the vehicle forebody become a significant section of the inlet compression process, whereas its afterbody performs a large part of the nozzle, which generates considerable thrust [35]. The propulsive system design encompasses the entire undersurface of the waverider. As a result, the engine and airframe become one [36]. In a real application, the periodic flight trajectory can be designed to widen the cruise range and to save the consumed energy [12]. For this reason, an illustrative example is provided for this study in a similar manner to the actual situation for waveriders [37].

Aerodynamic data are obtained for the geometry of the waverider in Figure 1 using a combination of oblique shock and Prandtl-Meyer flow theory in (51)-(56). The thrust is estimated based on the 1D Rayleigh flow scramjet propulsion model in (57)-(59). For simplicity, some shape parameters are suitably changeable in this study in comparison with those in [5] to ensure the rationality of the proposed model from the design viewpoint of flight control. When these model parameters are known, the polynomial expressions concerning these forces and moment can be identified. Additionally, we select the operation condition as $Ma = 8$, and $h = 27km$. The resulting aerodynamic and propulsive expressions are approximately acquired according to (65), and they are expressed below:

$$\begin{aligned} C_L(\alpha, \delta_e) &= -0.6107\alpha^2 + 2.1755\alpha + 0.0113 \\ &\quad + 0.2733 \times \delta_e \\ C_D(\alpha, \delta_e) &= 1.8934\alpha^2 + 0.0721\alpha + 0.0267 \\ C_M(\alpha, \delta_e) &= 2.4214\alpha^2 + 1.0467\alpha + 0.0878 - 0.9434 \\ &\quad \times \delta_e \\ \mathrm{T} &= 55108\Phi - 38159\alpha - 4680.8 \end{aligned} \tag{78}$$

Furthermore, the trim states in the vicinity of the operation condition based on (68) are plotted in Figure 4.

Figure 4 shows that the trim values dramatically change with the different flight Mach numbers and altitudes near the operation point, which demonstrates that the inherent dynamics of the waverider is sensitive to the change in the flight condition. Moreover, the flight dynamics is also unconventional due to the presence of the zero and pole in the right plane regarding (62), as displayed in Figure 5.

Figure 5 shows the zeros and poles on the right plane as the flight Mach number is changed from 7.8 to 8.2 and the altitude is changed from 26.5 km to 27.5 km. Obviously, these zeros and poles indicate that the nonlinear model of the waverider is unstable and a nonminimum phase as a result of the limitation for the control law design, such as the control bandwidth and effective control region. Furthermore, we select $\eta = 0.5$, $h_t = 27000m$, and $h_a = 300m$ in (69). The consumed fuel with the changes in the adjusted parameter r_f and flight range r is plotted in Figure 6.

According to (73) and (74), we can obtain the optimal adjusted parameter $r_f = 62931m$ by using the genetic algorithm. Thus, the reference command of the optimal periodic cruise in (73) is acquired as

$$\begin{aligned} h_c &= 27000 \\ &\quad + \exp\left[-0.5\left(\frac{r}{62931}\right)\right]\left[300\sin\left(\frac{2\pi r}{62931}\right)\right] \end{aligned} \tag{79}$$

The dynamic balance states can be solved by substituting (79) into (74). The results with the change in the flight range are provided in Figure 7.

Figure 7 demonstrates that the flight path angle, angle of attack, and control inputs change periodically to follow the expected flight trajectory in (79). Also, we consider the velocity change command with $\Delta V_c = 50m/s$ from $Ma = 8$ in the control process. In this case, W_1 and W_2 are selected as the unit matrix, and $F = \mathrm{diag}(F_1, F_2)$ is given as

$$\begin{aligned} F_1 &= \mathrm{diag}\,(1.2, 3.5, 10) \\ F_2 &= \mathrm{diag}\,(2, 4, 6, 6) \end{aligned} \tag{80}$$

The nonlinear gain functions ρ_1 and ρ_2 are selected as

$$\begin{aligned} \rho_1 &= -20\left|e^{-0.5|e_1|}\right| \\ \rho_2 &= -\left|e^{-0.2|e_2|}\right| \end{aligned} \tag{81}$$

In the simulation, the response results of the structures with CNF and without CNF are considered for the waverider model, passing through 200s. The results in relation to the steady-state flight and periodic cruise are presented in Figure 8.

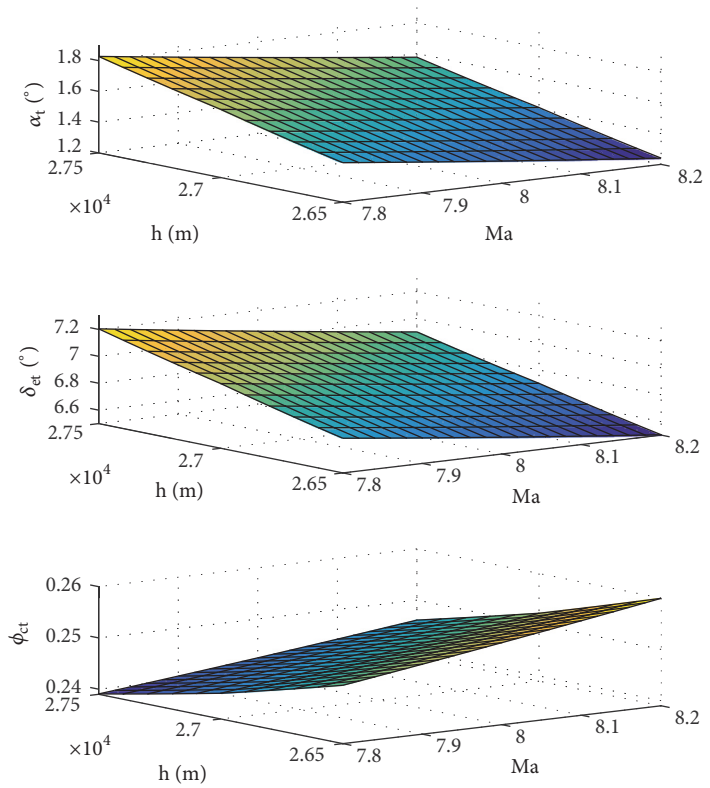

Figure 4: Change surfaces of trim values with regard to $Ma = 7.8 - 8.2$ and $h = 26.5km - 27.5km$.

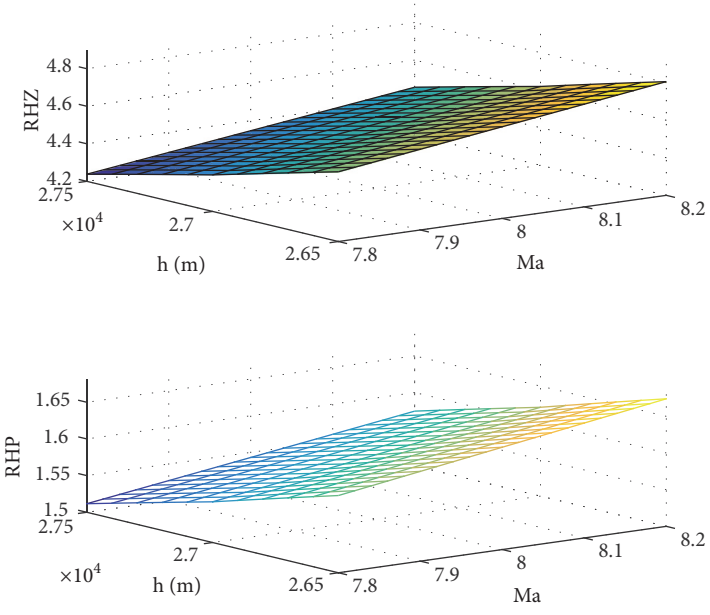

Figure 5: Change surfaces of zero and pole on the right plane with regard to $Ma = 7.8 - 8.2$ and $h = 26.5km - 27.5km$.

Figure 8 shows the contrast curves of the structures with CNF and without CNF. In consideration of the nonlinear part of the CNF control law in (21), the velocity and altitude output can rapidly follow the commands signals in contrast to that using only inversion control.

Figures 9 and 10 indicate the change curves of the angle of attack, flight path angle, and control inputs that gently return to the anticipated balance values due to the control action. Compared with the nonlinear control law provided in [38], the proposed controller which depends on

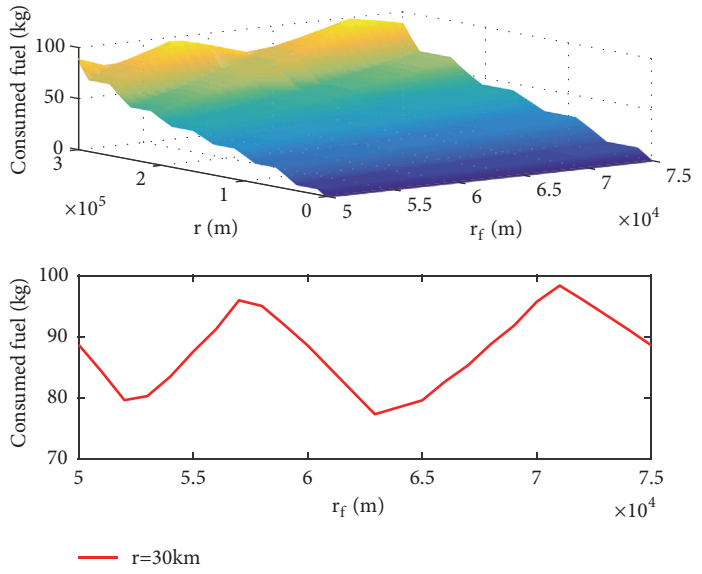

FIGURE 6: Consumed fuel with changes of adjusted parameter r_f and flight range r.

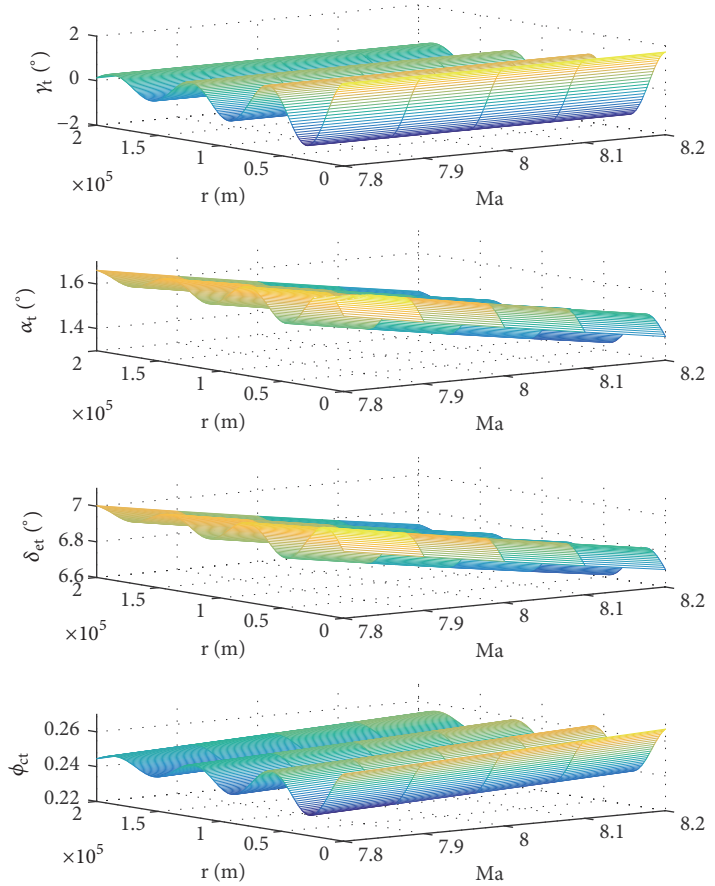

FIGURE 7: Change surfaces of dynamic balance states with regard to $Ma = 7.8 - 8.2$ and $r = 0km - 20km$.

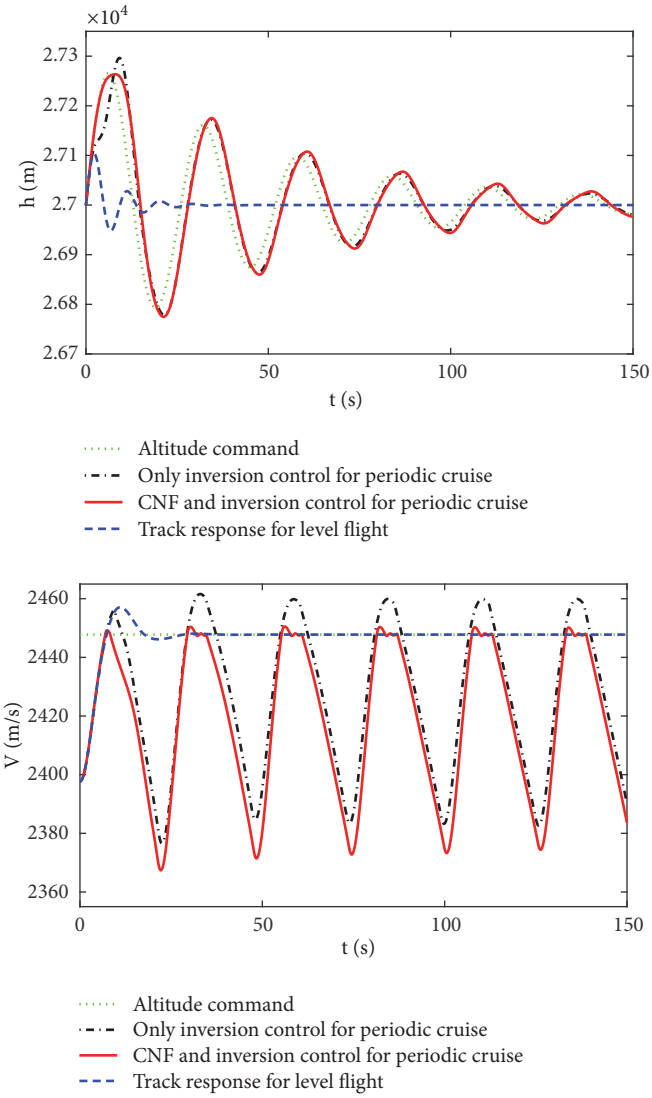

Figure 8: Response curves in relation to level flight and periodic cruise between with CNF and without CNF.

the nonlinear part of CNF makes the system outputs follow the periodic altitude command and step velocity command well while guaranteeing the control performances including small overshoot and fast settling time. In addition, the angle of attack is smaller using the CNF controller such that the propulsive force can keep stable and the drag can decrease accordingly. As a result, the consumed energy will reduce for the hypersonic vehicle due to the nonlinear part of CNF, and the transient performances will be improved for the periodic cruise trajectory of the hypersonic vehicle.

Figure 11 shows that the fuel consumed when flying with the periodic cruise trajectory is less than that flying with the steady-state cruise trajectory, whereas the consumed fuel using the CNF controller is minimal throughout the entire flight process. These results indicate that the flight control law using the CNF technique can not only improve the track performances but also achieve high fuel consumption savings for the waverider.

5. Conclusion

This study proposes a design method of the flight control law using the CNF technique to track the periodic cruise trajectory of the waverider. Compared with the well-known methods, the advantage of the proposed controller can guarantee the respected control qualities, including fast setting time, small overshot, and robustness over the hypersonic flight range. Furthermore, the simulation results show that the proposed control law improves the flight performance with input saturation. Fast setting time, small overshot, and robustness are ensured for the waverider while considering the tracking issue of the periodic cruise trajectory. However, we have assumed that all the flight states are available to feedback. Thus, future works should introduce the state observers for this presented control law so that these flight states can be estimated to satisfy the requirements in real applications.

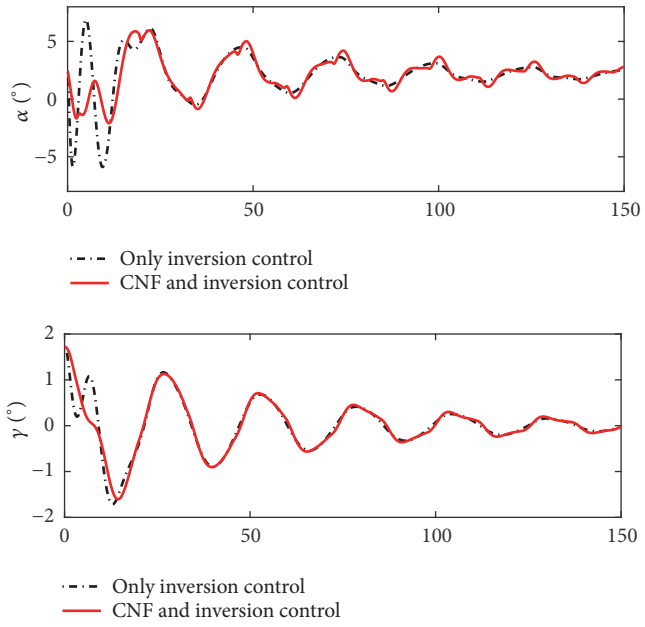

Figure 9: Angle of attack and flight path angle between with CNF and without CNF.

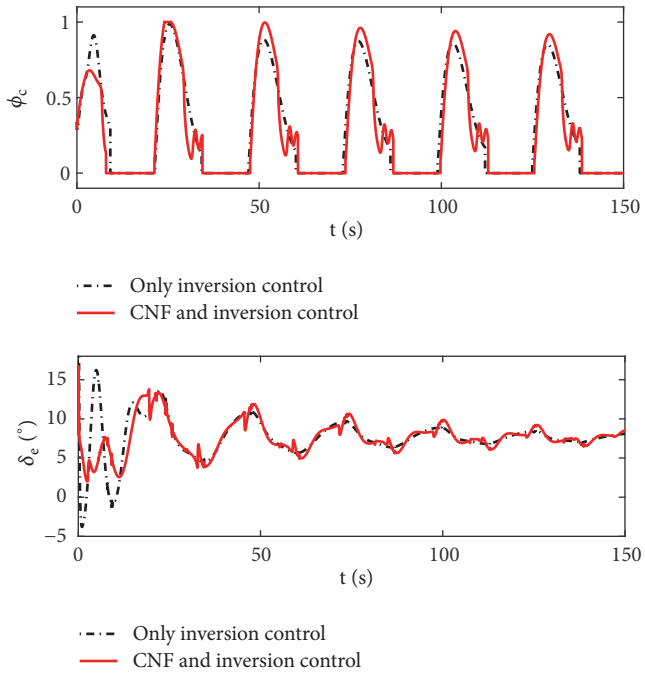

Figure 10: Control inputs between with CNF and without CNF.

Data Availability

The data used to support the findings of this study are included within the article.

Conflicts of Interest

The authors declare that there are no conflicts of interest regarding the publication of this article.

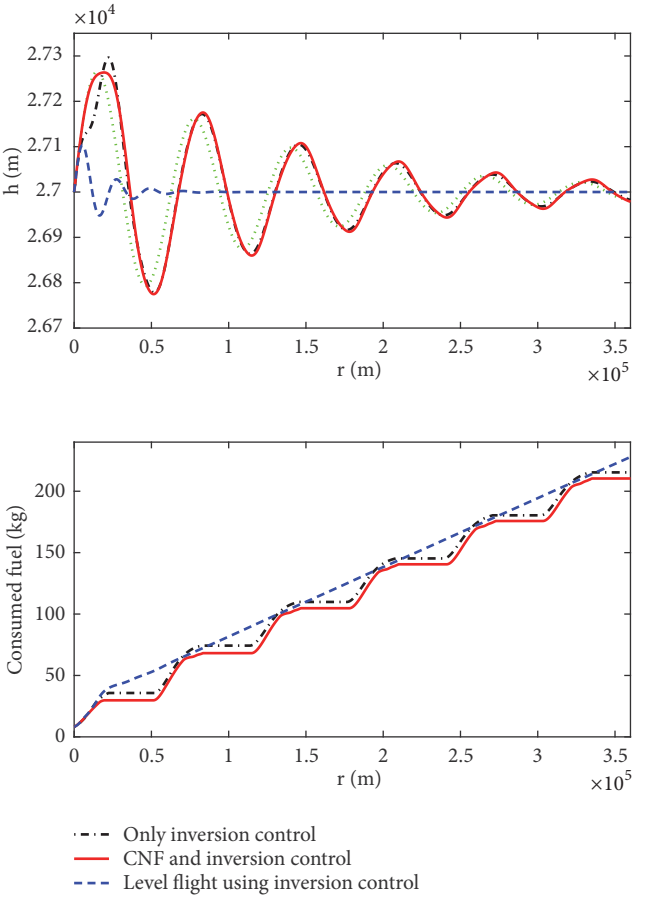

Figure 11: Consumed fuel in relation to level flight and periodic cruise between with CNF and without CNF.

Acknowledgments

This work is supported by Fundamental Research Funds for the Central Universities under Grant no. NZ2018008.

References

[1] X. Yin, X. Wei, L. Liu, and Y. Wang, "Improved hybrid fireworks algorithm-based parameter optimization in high-order sliding mode control of hypersonic vehicles," *Complexity*, vol. 2018, 16 pages, 2018.

[2] H. Duan and S. Li, "Artificial bee colony-based direct collocation for reentry trajectory optimization of hypersonic vehicle," *IEEE Transactions on Aerospace and Electronic Systems*, vol. 51, no. 1, pp. 615–626, 2015.

[3] F. R. Chavez and D. K. Schmidt, "Analytical aeropropulsive/aeroelastic hypersonic-vehicle model with dynamic analysis," *Journal of Guidance, Control, and Dynamics*, vol. 17, no. 6, pp. 1308–1319, 1994.

[4] C. Li, H. Wu, Z. Yang, Y. Wang, and Z. Sun, "A novel SHLNN based robust control and tracking method for hypersonic vehicle under parameter uncertainty," *Complexity*, vol. 2017, 14 pages, 2017.

[5] M. A. Bolender and D. B. Doman, "Nonlinear longitudinal dynamical model of an air-breathing hypersonic vehicle," *Journal of Spacecraft and Rockets*, vol. 44, no. 2, pp. 374–387, 2007.

[6] J. T. Parker, A. Serrani, S. Yurkovich, M. A. Bolender, and D. B. Doman, "Control-oriented modeling of an air-breathing hypersonic vehicle," *Journal of Guidance, Control, and Dynamics*, vol. 30, no. 3, pp. 856–869, 2007.

[7] S. G. V. Frendreis and C. E. S. Cesnik, "3-D simulation of flexible hypersonic vehicles," in *Proceedings of the AIAA Atmospheric Flight Mechanics Conference*, AIAA, Toronto, Canada, 2010.

[8] M. Shakiba and A. Serrani, "Control oriented modeling of 6-DOF hypersonic vehicle dynamics," in *Proceedings of the AIAA Guidance, Navigation and Control Conference 2011*, AIAA, Oregon, USA, August 2011.

[9] H. B. Sun, S. H. Li, and C. Y. Sun, "Finite time integral sliding mode control of hypersonic vehicles," *Nonlinear Dynamics*, vol. 73, no. 4, pp. 229–244, 2013.

[10] D. O. Sigthorsson, P. Jankovsky, A. Serrani, S. Yurkovich, M. A. Bolender, and D. B. Doman, "Robust linear output feedback control of an airbreathing hypersonic vehicle," *Journal of Guidance, Control, and Dynamics*, vol. 31, no. 4, pp. 1052–1066, 2008.

[11] D. A. Allwine, J. E. Fisher, J. A. Strahler, D. Lawrence, M. Oppenheimer, and D. Doman, "On-line trajectory generation for hypersonic vehicles," in *Proceedings of AIAA Guidance, Navigation, and Control Conference and Exhibit*, AIAA, San Francisco, Calif, USA, 2005.

[12] R. H. Chen, W. R. Williamson, J. L. Speyer, H. Youssef, and R. Chowdhry, "Optimization and implementation of periodic cruise for a hypersonic vehicle," *Journal of Guidance, Control, and Dynamics*, vol. 29, no. 3, pp. 1032–1040, 2006.

[13] J. T. Parker, A. Serrani, S. Yurkovich, M. A. Bolender, and D. B. Doman, "Approximate feedback linearization of an air-breathing hypersonic vehicle," in *Proceedings of AIAA Guidance, Navigation, and Control Conference and Exhibit*, AIAA, Keystone, CO, USA, August 2006.

[14] E. Rollins, J. Valasek, J. A. Muse, and M. A. Bolender, "Nonlinear adaptive dynamic inversion applied to a generic hypersonic vehicle," in *Proceedings of AIAA Guidance, Navigation, and Control (GNC) Conference*, AIAA, Boston, MA, USA, August 2013.

[15] L. Fiorentini, A. Serrani, M. A. Bolender, and D. B. Doman, "Nonlinear robust adaptive controller design for an air-breathing hypersonic vehicle model," *Journal of Guidance, Control, and Dynamics*, vol. 32, no. 2, pp. 401–416, 2009.

[16] Z. Lin, M. Pachter, and S. Banda, "Toward improvement of tracking performance: nonlinear feedback for linear systems," *International Journal of Control*, vol. 70, no. 1, pp. 1–11, 1998.

[17] M. C. Turner, I. Postlethwaite, and D. J. Walker, "Non-linear tracking control for multivariable constrained input linear systems," *International Journal of Control*, vol. 73, no. 12, pp. 1160–1172, 2000.

[18] B. M. Chen, T. H. Lee, K. Peng, and V. Venkataramanan, "Composite nonlinear feedback control for linear systems with input saturation: theory and an application," *IEEE Transactions on Automatic Control*, vol. 48, no. 3, pp. 427–439, 2003.

[19] K. Peng, B. M. Chen, G. Cheng, and T. H. Lee, "Modeling and compensation of nonlinearities and friction in a micro hard disk drive servo system with nonlinear feedback control," *IEEE Transactions on Control Systems Technology*, vol. 13, no. 5, pp. 708–721, 2005.

[20] W. Lan, B. M. Chen, and Y. He, "On improvement of transient performance in tracking control for a class of nonlinear systems with input saturation," *Systems & Control Letters*, vol. 55, no. 2, pp. 132–138, 2006.

[21] S. Mobayen and J. Ma, "Robust finite-time composite nonlinear feedback control for synchronization of uncertain chaotic systems with nonlinearity and time-delay," *Chaos Solitons and Fractals*, vol. 114, pp. 46–54, 2008.

[22] Y. He, B. M. Chen, and C. Wu, "Improving transient performance in tracking control for linear multivariable discrete-time systems with input saturation," *Systems and Control Letters*, vol. 56, no. 1, pp. 25–33, 2007.

[23] S. Mobayen and F. Tchier, "Composite nonlinear feedback control technique for master/slave synchronization of nonlinear systems," *Nonlinear Dynamics*, vol. 87, no. 3, pp. 1731–1747, 2017.

[24] S. Mobayen and F. Tchier, "Composite nonlinear feedback integral sliding mode tracker design for uncertain switched systems with input saturation," *Communications in Nonlinear Science and Numerical Simulation*, vol. 65, pp. 173–184, 2018.

[25] K. Peng and B. M. Chen, "Variant factor technique for tracking control of a class of nonlinear systems with input saturation," *Control and Intelligent Systems*, vol. 41, no. 3, pp. 169–177, 2013.

[26] J. Y. Choi, D. Chwa, and M.-S. Kim, "Adaptive control for feedback-linearized missiles with uncertainties," *IEEE Transactions on Aerospace and Electronic Systems*, vol. 36, no. 2, pp. 467–481, 2000.

[27] Q. Wang and R. F. Stengel, "Robust nonlinear flight control of a high-performance aircraft," *IEEE Transactions on Control Systems Technology*, vol. 13, no. 1, pp. 15–26, 2005.

[28] U. Mackenroth, *Robust Control Systems: Theory and Case Studies*, Springer-Verlag, Berlin, Germany, 2004.

[29] L. J. DeChant, "Effect of freestream velocity disturbances on hypersonic vehicles," *Journal of Spacecraft and Rockets*, vol. 49, no. 4, pp. 751–756, 2012.

[30] A. Clark, M. Mirmirani, S. Choi, C. Wu, and K. Mathew, "An aero-propulsion integrated elastic model of a generic airbreathing hypersonic vehicle," in *Proceedings of the AIAA Guidance, Navigation, and Control Conference and Exhibit*, AIAA, Keystone, CO, USA, 2006.

[31] C. E. Whitmer, A. G. Kelkar, J. M. Vogel, D. S. Chaussee, and C. J. Ford, "Control centric parametric trade studies for scramjet-powered hypersonic vehicles," in *Proceedings of AIAA Guidance, Navigation, and Control Conference and Exhibit*, Toronto, Canada, August 2010.

[32] Y. Liu, J. Deng, and Y. Lu, "Preliminary research on optimal design based on control demands for hypersonic morphing vehicle," *IEEE Aerospace and Electronic Systems Magazine*, vol. 28, no. 5, pp. 23–31, 2013.

[33] M. A. Bolender and D. B. Doman, "Flight path angle dynamics of air-breathing hypersonic vehicles," in *Proceedings of the AIAA Guidance, Navigation, and Control Conference and Exhibit*, AIAA, Keystone, CO, USA, August 2006.

[34] L. E. Rudd, D. J. Pines, and P. H. Carter, "Long-range performance of suboptimal periodic hypersonic cruise trajectories," *Journal of Guidance Control and Dynamics*, vol. 23, no. 4, pp. 756–758, 2000.

[35] L. Liu, S. Dong, Y. Wang, and L. Ou, "Clearance of flight control law based on structural singular value theory," *IEEE Transactions on Aerospace and Electronic Systems*, vol. 51, no. 3, pp. 2138–2147, 2015.

[36] J. J. Dickeson, A. A. Rodriguez, S. Sridharan, and A. Korad, "Elevator sizing, placement, and control-relevant tradeoffs for hypersonic vehicles," in *Proceedings of AIAA Guidance, Navigation, and Control Conference*, AIAA, Toronto, Canada, August 2010.

[37] P. H. Carter II, D. J. Pines, and L. VonEggers Rudd, "Approximate performance of periodic hypersonic cruise trajectories for global reach," *Journal of Aircraft*, vol. 35, no. 6, pp. 857–867, 1998.

[38] J. Parker, A. Serrani, S. Yurkovich, M. Bolender, and D. Doman, "Approximate feedback linearization of an air-breathing hypersonic vehicle," in *Proceedings of the AIAA Guidance, Navigation, and Control Conference and Exhibit*, Keystone, CO, USA, 2006.